Simultaneous Extension and Shear Piezoelectric Actuation for Active Vibration Control of Sandwich Beams

Marcelo A. Trindade

Journal of Intelligent Material Systems and Structures 2007; 18; 591 originally published online Jan 22, 2007;
DOI: 10.1177/1045389X06076592

Simultaneous Extension and Shear Piezoelectric Actuation for Active Vibration Control of Sandwich Beams

MARCELO A. TRINDADE*

Department of Mechanical Engineering, São Carlos School of Engineering, University of São Paulo, Av. Trabalhador São-Carlense, 400, 13566-590, São Carlos, SP, Brazil

ABSTRACT: Piezoelectric materials are widely used as distributed means for sensing and/or actuating a structure's response, either by bonding them to the surfaces of a structure or embedding them into a laminate structure. Surface-mounted actuators are normally poled in thickness direction so that they work in the extension mode, while embedded actuators are more effective when poled in the longitudinal direction and thus working in the thickness-shear mode. It has been shown that embedded shear actuators may lead to less problems of actuators damage and debonding, minor dependence on actuators position, and length and smaller stresses in the actuators. It has also been observed that the surface-mounted extension actuators are generally more effective for very flexible host structures while embedded shear actuators are more effective for stiffer structures. These and other distinctive features of extension and shear actuators may be exploited to study their simultaneous use and to design a combined extension–shear actuated beam. Hence, this work presents the results of a numerical investigation of active vibration control using simultaneous extension and shear piezoelectric actuation for a clamped–clamped sandwich beam. The analysis is carried out using a laminate/sandwich beam finite element model combined to an optimal control with limited input. Results show that simultaneous use of extension and shear actuators is very promising since their actuation mechanisms are complementary. In particular, a good damping performance was obtained over an increased frequency-range with very localized actuators.

Key Words: vibration control, piezoelectric materials, shear actuators, embedded actuators, sandwich beams.

INTRODUCTION

WHEN incorporated into a laminated composite structure, piezoelectric materials can be used as distributed means for sensing and/or actuating the structure's response. This is achieved thanks to the electromechanical interaction that occurs in a piezoelectric material for which the application of a force or pressure produces electric charge/voltage (direct piezoelectric effect) and the application of electric charge/voltage is responded by induced strain (converse piezoelectric effect). Therefore, the dynamic response of a structure with incorporated piezoelectric layers/patches can be both monitored, through the measure of the charge/voltage induced in the piezoelectric element(s) acting as sensor(s), and controlled, through the application of an appropriate charge/voltage to the piezoelectric element(s) acting as actuator(s). It is clear that to effectively control the structure's response using piezoelectric sensors and actuators, one must not only be able to sense and actuate the structure's response but also evaluate the appropriate charge/voltage to be applied to the actuator(s) based on the measured charge/voltage induced in the sensor(s). This is achieved by a control system that connects the sensor(s) and actuator(s) and can be designed to induce the required response to the structure.

Over the past two decades, several research works have shown that the use of integrated piezoelectric patches acting as sensors and/or actuators allows effective control of the structure's vibrations (Sunar and Rao, 1999). These laminated composite structures with integrated piezoelectric sensors and actuators form a class of 'smart structures' that has been widely used for structural vibration control in recent years. The piezoelectric layers/patches can either be bonded to the surfaces of the host structure or embedded into a laminate structure. Surface-bonded, also known as surface-mounted, actuators have the advantage of ease in construction, access, and maintainability but may be subjected to high longitudinal stresses and contact with surrounding objects that may be detrimental to normally brittle piezoceramic materials. Embedding the piezoelectric layers/patches alleviate these problems and also enables good mechanical and electrical link

*E-mail: trindade@sc.usp.br

Figures 3, 4, 9, and 10 appear in color online: http://jim.sagepub.com

1045-389X/07/06 0591–10 $10.00/0 DOI: 10.1177/1045389X06076592

with the structural element, and gluing materials may be unnecessary. On the other hand, embedding may lead to complex manufacturing and electrical insulation.

Surface-mounted piezoelectric actuators are normally poled in the thickness direction so that the application of a through-thickness electric field forces an elongation or contraction of the actuators. If the actuators are well-bonded to the surface of the host structure, their elongation or contraction causes a deformation of the host structure. This may be represented as the application of axial forces on the structure's surface at the actuator edges leading to bending moments applied to the structure's neutral line. Hence, the surface-mounted actuators are also known as extension or extension-bending actuators. They have widely been used on active (Sunar and Rao, 1999), passive (Ahmadian and DeGuilio, 2001), and hybrid active–passive (Trindade and Benjeddou, 2002) control applications. Although extension actuators can be very effective when surface-mounted on the host structure, they are not very effective when embedded in a laminate structure. This is because they induce smaller bending moments when they are close to the structure's neutral line.

A recent work of Sun and Zhang (1995) proposed the use of the thickness-shear mode of piezoelectric actuators embedded in a sandwich beam. In this case, the piezoelectric patches are poled in the axial direction and, when subjected to the standard through-thickness electric field, induce thickness shear stress in the sandwich structure's core. These piezoelectric actuators are known as shear actuators and are produced by some piezoceramic manufacturers normally in the form of plates poled in the length or width direction. Sun and Zhang (1995) and Zhang and Sun (1996) have shown that embedded shear actuators are subjected to lower stresses, under actuation. Through the use of a classical sandwich beam theory, Benjeddou et al. (1997, 1999, 2000) showed that shear actuators induce distributed actuation moments in the structure unlike extension actuators which induce boundary forces. Therefore, shear actuation mechanism may lead to less problems of debonding in actuator boundaries and to a minor dependence of the control performance on the actuators position and length. Aldraihem and Khdeir (2000, 2003) and Khdeir and Aldraihem (2001) presented exact solutions for sandwich beams with shear and extension actuators using equivalent single layer models based on first-order and third-order shear deformation theories. Trindade et al. (1999) presented a comparison between the active control performances of shear and extension actuation mechanisms using a sandwich beam finite element model. They showed that shear actuators are generally more suitable to control bending vibrations of stiff structures. Raja et al. (2002) also studied active damping performance in composite materials using shear actuators as compared to using the widespread extension actuators. Their results showed that shear actuators have promising features for vibration control applications. In particular the shear actuator was observed to be more effective in velocity feedback than the extension actuator. In a later work, Raja et al. (2004) presented a finite element static analysis of sandwich beams actuated simultaneously by shear and extension actuators for several boundary conditions. Recent experiments and numerical simulations performed by Baillargeon and Vel (2005) have shown that shear actuators can provide a significant reduction on the vibrations of a sandwich beam. Vel and Batra (2001) presented an exact 3D solution for the static cylindrical bending of simply supported laminated plates with embedded shear piezoelectric actuators. Their analysis has shown that both longitudinal and shear stresses within the actuator are significantly smaller for the shear actuator. Edery-Azulay and Abramovich (2004) also presented closed-form solutions for the static analysis of laminate/sandwich beams with embedded extension and shear actuators.

In some of the aforementioned studies, it has been observed that extension actuators are generally more effective for very flexible host structures while shear actuators are more effective for stiffer structures (e.g. short beams). Also, the effectiveness of extension actuators is more dependent on the position along the beam than shear actuators. These and other distinctive features of extension and shear actuators may be exploited to study their simultaneous use and to design a combined extension-shear actuated beam. Hence, this work presents the results of a numerical investigation of active vibration control using simultaneous extension and shear piezoelectric actuation for a clamped–clamped sandwich beam. The analysis is carried out using a laminate/sandwich beam finite element model joined to an optimal control with limited input.

THEORETICAL FORMULATION

A multilayer sandwich beam, with elastic and/or piezoelectric layers, is considered. One of the layers is allowed to perform membrane, bending, and shear strains and is known as a core layer. Thus, one may denote the upper and lower layers, relative to the core, as face sub-layers. These undergo only membrane and bending strains and hence are modeled using classical laminate theory. This leads to a classical sandwich theory (face/core/face) with laminate faces. Euler–Bernoulli assumptions are considered for the laminate faces whereas, those of Timoshenko are retained for the core. The piezoelectric face sub-layers are supposed to be transversely poled and subject to transverse electric fields. On the contrary, the piezoelectric core layer is supposed to be longitudinally

poled but also subject to transverse electric fields. Elastic layers are assumed to be insulated and are obtained by annulling the piezoelectric constants. All layers are assumed to be in plane stress state and are perfectly bonded, using a nonconductive bonding layer such that the electric state of each layer can be independent of its adjacent layers. The length, width, and thickness of the beam are denoted by L, b, and h, respectively. The subscripts a_j, b_j, and c refer to quantities relative to the j-th sub-layer of upper a and lower b faces and to the core, respectively. More details on the formulation can be found in a previous work (Trindade et al., 2001).

Strains and Electrical Fields

As stated before, classical sandwich beam theory is used here. This means that the same displacement field u_k $(k = a, b)$ is considered for all sub-layers k_j of the laminate face k. Hence, despite the number n and m of sub-layers in the faces a and b respectively, only three displacement fields may be considered. Axial displacements $u_i(x, y, z)$ of the i-th layer $(i = a, b, c)$ are assumed to vary in x-direction, vanish in y-direction, and be linear in z-direction (through thickness). As for the transverse deflections $w_i(x, y, z)$, they are supposed to vary only in x-direction. From Euler–Bernoulli hypotheses, the cross-section rotation of the faces β_k $(k = a, b)$ is related to the deflection derivative w' as $\beta_k = -w'$, where w' is used to denote $\partial w/\partial x$. The mid-plan of the core is set to coincide with the origin of the z-axis. Then, using the displacement continuity conditions between layers, the axial and shear strains of the i-th layer $(i = a, b, c)$ can be written in terms of the transverse deflection w and the mean and relative axial displacements of the laminate faces $\bar{u} = (u_a + u_b)/2$ and $\tilde{u} = u_a - u_b$. Hence, the axial ε_1 and shear ε_5 strains are written as

$$\varepsilon_{1i} = \varepsilon_i^m + (z - z_i)\varepsilon_i^b \ , \quad \varepsilon_{5i} = \varepsilon_i^s \tag{1}$$

where

$$\varepsilon_a^m = \bar{u}' + \frac{\tilde{u}'}{2}, \quad \varepsilon_b^m = \bar{u}' - \frac{\tilde{u}'}{2}, \quad \varepsilon_c^m = \bar{u}' + dw'',$$

$$\varepsilon_a^b = -w'', \qquad \varepsilon_b^b = -w'', \qquad \varepsilon_c^b = \frac{\tilde{u}'}{h_c} + \lambda w'',$$

$$\varepsilon_a^s = 0, \qquad \varepsilon_b^s = 0, \qquad \varepsilon_c^s = \frac{\tilde{u}}{h_c} + (\lambda + 1)w',$$

and

$$d = (h_a - h_b)/4, \ \lambda = (h_a + h_b)/2h_c,$$

$$z_k = \pm(h_k + h_c)/2, \ h_k = \sum_{j=1}^{n,m} h_{k_j}.$$

These generalized strains ε_i^m, ε_i^b, and ε_i^s define the membrane, bending, and shear strains of each layer.

A constant transverse electrical field is assumed for the piezoelectric layers and the remaining in-plane components are supposed to vanish. Consequently it is, for the k_j-th face piezoelectric sub-layer and core c,

$$E_{3k_j} = -\frac{V_{k_j}}{h_{k_j}} \ ; \quad E_{3c} = -\frac{V_c}{h_c} \tag{2}$$

where V_{k_j} and V_c are the difference of electric potential of the k_j-th and c laminae, defined by $V_{k_j} = V_{k_j}^+ - V_{k_j}^-$ and $V_c = V_c^+ - V_c^-$, where $V_{k_j}^+, V_c^+$ and $V_{k_j}^-, V_c^-$ are the voltages applied on the upper and lower skins of the k_j-th face and core c piezoelectric sub-layer.

Reduced Constitutive Equations

Linear orthotropic piezoelectric materials with material symmetry axes parallel to those of the beam are considered. c_{ij}, e_{lj}, and ε_{ll} $(i, j = 1, ..., 6; l = 1, 2, 3)$ denote their elastic, piezoelectric, and dielectric constants. For simplicity of notation, all layers will be considered piezoelectric. Elastic layers are obtained by making their piezoelectric constants vanish.

The three-dimensional linear constitutive equations of an orthotropic piezoelectric layer, poled in the thickness direction, can be reduced as (Benjeddou et al., 1997)

$$\begin{Bmatrix} \sigma_{1k_j} \\ D_{3k_j} \end{Bmatrix} = \begin{bmatrix} c_{11}^{*k_j} & -e_{31}^{*k_j} \\ e_{31}^{*k_j} & \epsilon_{33}^{*k_j} \end{bmatrix} \begin{Bmatrix} \varepsilon_{1k} \\ E_{3k_j} \end{Bmatrix} \tag{3}$$

where

$$\epsilon_{33}^{*k_j} = \epsilon_{33}^{k_j} + \frac{{e_{33}^{k_j}}^2}{c_{33}^{k_j}} \ , \ e_{31}^{*k_j} = e_{31}^{k_j} - \frac{c_{13}^{k_j}}{c_{33}^{k_j}} e_{33}^{k_j} \ , \ c_{11}^{*k_j} = c_{11}^{k_j} - \frac{{c_{13}^{k_j}}^2}{c_{33}^{k_j}}$$

while σ_{1k_j} and D_{3k_j} are axial stress components and transverse electrical displacement. Notice that electromechanical coupling in the piezoelectric faces sub-layers is between axial strain and transverse electrical field.

The piezoelectric material considered for the core is poled in the longitudinal direction. Hence, its constitutive equations may be obtained by a rotation of the three-dimensional constitutive equations of an orthotropic piezoelectric layer such that the directions x and z interchange. Thereafter, using the plane stress assumption, they can be reduced to

$$\begin{Bmatrix} \sigma_{1c} \\ \sigma_{5c} \\ D_{3c} \end{Bmatrix} = \begin{bmatrix} c_{33}^{*c} & 0 & 0 \\ 0 & c_{55}^{c} & -e_{15}^{c} \\ 0 & e_{15}^{c} & \epsilon_{11}^{c} \end{bmatrix} \begin{Bmatrix} \varepsilon_{1c} \\ \varepsilon_{5c} \\ E_{3c} \end{Bmatrix} \tag{4}$$

where

$$c_{33}^{*c} = c_{33}^{c} - \frac{{c_{13}^{c}}^2}{c_{11}^{c}}.$$

The axial electrical field E_{1c} is coupled with the axial strain of the core. However, its contribution to the electromechanical energy is neglected here, since only bending vibration is of interest. One may notice that the electromechanical coupling is between the transverse electrical field and the shear strains.

Variational Formulation

From constitutive Equations (3) and (4), the virtual work of electromechanical internal forces of the piezoelectric multilayer/sandwich beam may be written as

$$\delta H = \delta H_c + \sum_{k=a}^{b} \sum_{j=1}^{n,m} \delta H_{k_j} \tag{5}$$

where, over the volume Ω_{k_j} and Ω_c,

$$\begin{aligned} \delta H_{k_j} &= \int_{\Omega_{k_j}} \left(\sigma_{1k_j}\delta\varepsilon_{k1} - D_{3k_j}\delta E_{3k_j}\right) \mathrm{d}\Omega_{k_j} \\ \delta H_c &= \int_{\Omega_c} (\delta\varepsilon_{1c}\sigma_{1c} + \delta\varepsilon_{5c}\sigma_{5c} - \delta E_{3c}D_{3c}) \mathrm{d}\Omega_c. \end{aligned} \tag{6}$$

Then, together with the virtual work of inertial δT and applied mechanical forces δW, described in detail in a previous work (Trindade et al., 2001), the D'Alembert's principle extended to piezoelectric media may be written as

$$\delta T - \delta H + \delta W = 0 \; ; \quad \forall\, \delta\bar{u}, \delta\tilde{u}, \delta w, \delta V_{k_j}, \delta V_c. \tag{7}$$

FINITE ELEMENT FORMULATION

From the variational formulation, and using strain and electrical field, described in the last section, a finite element model was developed for the laminate faces adaptive sandwich beam. It assumes Lagrange linear shape functions for the mean and relative axial displacements, $\bar{u}$ and $\tilde{u}$ and Hermite cubic ones for the transverse deflection w. The difference of electric potentials V_{k_r} $(r = 1, \ldots, (N, M))$ and V_c of the N, M face piezoelectric sub-layers and core c are assumed constant in the element (Figure 1). This leads to the following elementary degrees of freedom (dof) column vector $\hat{\mathbf{q}}_e$,

$$\begin{aligned} \hat{\mathbf{q}}_e = \mathrm{col}(&\bar{u}_1, w_1, w_1', \tilde{u}_1, \bar{u}_2, w_2, w_2', \tilde{u}_2, \\ &V_{a_1}, \ldots, V_{a_N}, V_{b_1}, \ldots, V_{b_M}, V_c). \end{aligned} \tag{8}$$

Assembling on the faces sub-layers, then on the beam layers, the discretized variational Equation (7) reduced to the element level can be written as,

$$(\mathbf{M}_f^e + \mathbf{M}_c^e)\ddot{\hat{\mathbf{q}}}_e + (\mathbf{K}_f^e + \mathbf{K}_c^e)\hat{\mathbf{q}}_e = \mathbf{F}_m^e \tag{9}$$

where $\mathbf{M}_f^e = \sum_k \sum_j \mathbf{M}_{k_j}^e$ and $\mathbf{K}_f^e = \sum_k \sum_j \mathbf{K}_{k_j}^e$. One may notice that, since electrical dof inertia vanishes, mechanical and electrical dof are coupled only statically (time-independent relationship). Therefore, two different cases may be considered for each piezoelectric sub-layer: applied difference of potentials (actuator) or unknown difference of potentials (sensor). Let the corresponding subgroups be defined as $\mathbf{V}_A^e$ and $\mathbf{V}_S^e$ of the elementary electrical dof $\mathbf{V}^e$. Then, the vector $\hat{\mathbf{q}}_e$ in Equation (8) may be decomposed such that $\hat{\mathbf{q}}_e = (\mathbf{q}_e, \mathbf{V}_S^e, \mathbf{V}_A^e)$. Consequently, Equation (9) becomes

$$\begin{aligned} &\begin{bmatrix} \mathbf{M}^e & \mathbf{0} & \mathbf{0} \\ \mathbf{0} & \mathbf{0} & \mathbf{0} \\ \mathbf{0} & \mathbf{0} & \mathbf{0} \end{bmatrix} \begin{Bmatrix} \ddot{\mathbf{q}}_e \\ \ddot{\mathbf{V}}_S^e \\ \ddot{\mathbf{V}}_A^e \end{Bmatrix} \\ &\quad + \begin{bmatrix} \mathbf{K}_m^e & -\mathbf{K}_{meS}^e & -\mathbf{K}_{meA}^e \\ -\mathbf{K}_{meS}^{e\,T} & \mathbf{K}_{eS}^e & \mathbf{0} \\ -\mathbf{K}_{meA}^{e\,T} & \mathbf{0} & \mathbf{K}_{eA}^e \end{bmatrix} \begin{Bmatrix} \mathbf{q}_e \\ \mathbf{V}_S^e \\ \mathbf{V}_A^e \end{Bmatrix} = \begin{Bmatrix} \mathbf{F}_m^e \\ \mathbf{0} \\ \mathbf{0} \end{Bmatrix}. \end{aligned} \tag{10}$$

Since the electrical dofs $\mathbf{V}_A^e$ are imposed, their virtual variations $\delta\mathbf{V}_A^e$ vanish. Therefore, the third line of Equation (10) is automatically satisfied and may be ignored. Also the corresponding term to $\mathbf{V}_A^e$ in the first equation can be moved to the right-hand side as an equivalent electrical work, defined by

$$\mathbf{F}_e^e = \mathbf{K}_{meA}^e \mathbf{V}_A^e. \tag{11}$$

The second line of Equation (10) can then be used to express the unknown potentials $\mathbf{V}_S^e$ in terms of the mechanical dof $\mathbf{q}_e$, such as

$$\mathbf{V}_S^e = \mathbf{K}_{eS}^{e\,-1} \mathbf{K}_{meS}^{e\,T} \mathbf{q}_e. \tag{12}$$

Replacing Equations (11) and (12) in the first line of Equation (10) leads to the following electrical dof condensed elementary system which is given by

$$\mathbf{M}^e\ddot{\mathbf{q}}_e + \left(\mathbf{K}_m^e - \mathbf{K}_{meS}^e \mathbf{K}_{eS}^{e\,-1} \mathbf{K}_{meS}^{e\,T}\right)\mathbf{q}_e = \mathbf{F}_m^e + \mathbf{F}_e^e. \tag{13}$$

Hence, the mechanical dof, due to mechanical and/or electrical loads $\mathbf{F}_m^e$ and $\mathbf{F}_e^e$, may be evaluated first,

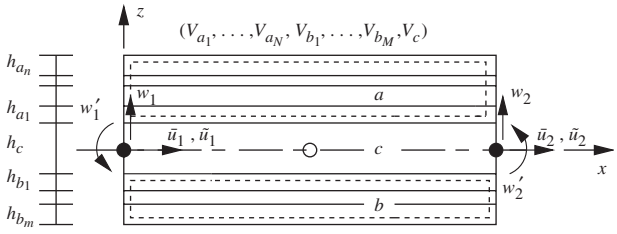

Figure 1. *Piezoelectric laminated sandwich beam finite element.*

then unknown electrical dof are found through a post-processing calculation using Equation (12). This method not only leads to faster calculations since matrices dimensions are lower but also prevents ill-conditioning problems of solving Equation (10) directly. Therefore, both piezoelectric actuators and sensors can be considered in a closed-loop analysis.

Then, one may assemble this elementary system to get the corresponding global mass and stiffness matrices, and mechanical and electrical load vectors, $\mathbf{M}$, $\mathbf{K}_f$, $\mathbf{K}_c$, $\mathbf{F}_m$, and $\mathbf{F}_e$. Also, a standard viscous damping matrix $\mathbf{D}$ may be considered *a posteriori* to represent all forms of damping apart from the one induced by piezoelectric active control. Consequently, the assembled system becomes

$$\mathbf{M}\ddot{\mathbf{q}} + \mathbf{D}\dot{\mathbf{q}} + (\mathbf{K}_f + \mathbf{K}_c)\mathbf{q} = \mathbf{F}_m + \mathbf{F}_e. \tag{14}$$

MODEL REDUCTION

In order to apply the equations of motion to control design, a model reduction is normally required. Here, Equation (14) is reduced through projection on a truncated modal basis Φ such that the finite element dof vector $\mathbf{q}$ are approximated by $\mathbf{q} = \Phi\chi$, with χ being the modal displacements. Thus, Equation (14) may be rewritten as

$$\ddot{\chi} + 2\zeta\Omega\dot{\chi} + \Omega^2\chi = \mathscr{F}_m + \mathscr{F}_e \tag{15}$$

where the eigenvectors Φ are mass-normalized such that $\Phi^T\mathbf{M}\Phi = \mathbf{I}$ and Ω states for the undamped eigenfrequencies matrix. The damping matrix $\mathbf{D}$ is chosen such that the resulting projected modal damping matrix is diagonal and proportional to the eigenfrequencies matrix and ζ defines a modal damping factor equal for all the modes considered. Then, one gets

$$\Omega^2 = \Phi^T(\mathbf{K}_f + \mathbf{K}_c)\Phi. \tag{16}$$

Notice that these eigenfrequencies already account for induced electric fields in the piezoelectric sensor layers. The modal perturbation and control forces contributions are obtained through projection of $\mathbf{F}_m$ and $\mathbf{F}_e$ in the modal basis Φ,

$$\mathscr{F}_m = \Phi^T\mathbf{F}_m\ ; \qquad \mathscr{F}_e = \Phi^T\mathbf{F}_e. \tag{17}$$

The projection of piezoelectric control forces $\mathbf{F}_e$ in the modal basis presents an important meaning for control design. This is because the magnitude of the elements of $\mathcal{F}_e$ represents a measure of the controllability of the corresponding mode. Hence, the greater the projection of $\mathbf{F}_e$ for a given mode, the greater is the ability of this force to control this mode.

For control design, the second-order Equation (15) is transformed into state-space form as follows

$$\begin{aligned}\dot{\mathbf{x}} &= \mathbf{A}\mathbf{x} + \mathbf{B}\mathbf{u} + \mathbf{p}\\ \mathbf{y} &= \mathbf{C}\mathbf{x}\end{aligned}, \qquad \text{with } \mathbf{x} = \begin{Bmatrix}\chi\\ \dot{\chi}\end{Bmatrix}. \tag{18}$$

The output variables vector $\mathbf{y}$ is written as combinations of the state variables, through matrix $\mathbf{C}$. However, the state variables, that are modal displacements χ and velocities $\dot{\chi}$, are difficult to measure. Nevertheless, as these may be expressed in terms of the finite element dof and their derivatives, one may consider an output vector $\mathbf{y} = \mathbf{C}_p\mathbf{q} + \mathbf{C}_d\dot{\mathbf{q}}$, so that the matrices $\mathbf{C}_p$ and $\mathbf{C}_d$ allow the measurement of nodal displacements and velocities. Then, the output matrix $\mathbf{C}$ may be written in terms of $\mathbf{C}_p$ and $\mathbf{C}_d$ shown as follows. Similarly, $\mathbf{A}$, $\mathbf{B}$ and $\mathbf{p}$, which are the system dynamics, input distribution, and perturbation matrices, respectively, are given by

$$\begin{aligned}&\mathbf{A} = \begin{bmatrix}\mathbf{0} & \mathbf{I}\\ -\Omega^2 & -2\zeta\Omega\end{bmatrix};\ \mathbf{B} = \begin{bmatrix}\mathbf{0}\\ \mathcal{F}_e^*\end{bmatrix};\ \mathbf{p} = \begin{bmatrix}\mathbf{0}\\ \mathcal{F}_m\end{bmatrix};\\ &\mathbf{C} = \begin{bmatrix}\mathbf{C}_p\Phi\ \mathbf{C}_d\Phi\end{bmatrix}.\end{aligned} \tag{19}$$

To account for the control input $\mathbf{u}$, which is here the voltage applied to the actuators, the input distribution matrix $\mathbf{B}$ is written in terms of a potential factored-out piezoelectric force vector $\mathcal{F}_e^*$. This is defined as the piezoelectric force $\mathcal{F}_e$ for a unit applied voltage on the corresponding actuator.

CONTROL DESIGN

The state-space system Equation (18) is now applied to the design of an optimal controller. The control algorithm considered here is an iterative version of the linear quadratic regulator (LQR) in order to find an optimal linear feedback controller while respecting a prescribed maximum voltage applied to the piezoelectric actuators to prevent their depoling. Hence, a full state feedback control $\mathbf{u} = -\mathbf{K}_g\mathbf{x}$ is considered to minimize the functional

$$J = \frac{1}{2}\int_0^\infty (\mathbf{x}^T\mathbf{Q}\mathbf{x} + \mathbf{u}^T\mathbf{R}\mathbf{u})\ \mathrm{d}t \tag{20}$$

subjected to the linear constraints of Equation (18) and to the voltage limitation $\mathbf{u} < V_{\max}$. Evidently, the performance of this controller depends on the state $\mathbf{Q}$ and input $\mathbf{R}$ weight matrices, where $\mathbf{Q}$ defines the relative weight of each state variable and $\mathbf{R}$ defines the relative weight of each actuator voltage. The latter is supposed to be in the form $\mathbf{R} = \gamma\,\mathbf{I}$ and the factor γ is then adjusted automatically to limit the maximum voltage, through an iterative algorithm. Consequently, the control gain matrix $\mathbf{K}_g = \mathbf{R}^{-1}\mathbf{B}^T\mathbf{P}$ is evaluated,

for each value of γ, by solving for $\mathbf{P}$ the following algebraic Riccati equation

$$\mathbf{A}^T\mathbf{P} + \mathbf{P}\mathbf{A} - \mathbf{P}\mathbf{B}\mathbf{R}^{-1}\mathbf{B}^T\mathbf{P} + \mathbf{Q} = \mathbf{0}. \qquad (21)$$

It is clear that the computational cost of this iterative algorithm increases greatly with the dimension of the state-space system. However, the convergence is generally very fast. One may also notice that the maximum control voltage must be evaluated in terms of the dynamics of the system for a given perturbation. Hence, the voltage limitation leads to a perturbation-dependent performance of the controller.

NUMERICAL RESULTS AND DISCUSSION

The reduced model together with the control algorithm are now used to investigate the active damping performances of extension, shear, and combined extension–shear actuation mechanisms. For that, consider the clamped–clamped sandwich beam with two facing layers made of steel and one core made of foam as shown in Figure 2. The material and geometrical properties of the sandwich beam are shown in Table 1. This host structure may be controlled by bonding the extension actuators in its surfaces and/or by inserting shears actuators in the sandwich core, replacing the existing foam. Here, it is proposed to integrate two extension and/or shear actuators at opposite sides of the clamped–clamped sandwich beam as shown in Figure 2. This is an interesting configuration since many practical cases require the actuators located near the clamped end and it is well-known that single extension actuators are more effective near the center of a clamped–clamped beam. However, through static and dynamic analyses, it is shown later in this work that a pair of extension and shear actuators located near the clamped ends can be effective as well. First, a static analysis is carried out to better understand the actuation mechanisms of extension and shear piezoelectric actuators. Then, a selected configuration is combined with the control algorithm to evaluate the active damping performance of extension, shear, and combined extension–shear actuators.

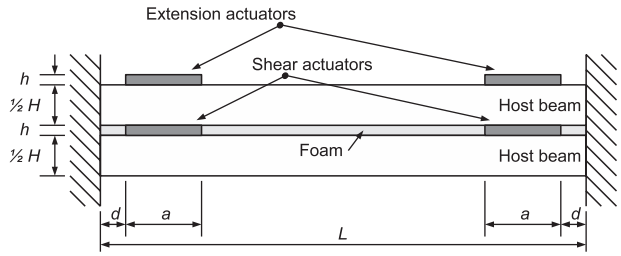

Figure 2. *Clamped–clamped sandwich beam with extension and shear actuators.*

Table 1. *Material and geometrical properties.*

Geometrical properties (in mm)
$L = 320$, $H = 5$, $h = 0.5$, $d = 10$, $a = 33$

Material properties (*Steel host beam*)
$\rho = 7800\,\mathrm{kg\,m^{-3}}$, $E = 210\,\mathrm{GPa}$

Foam
$\rho = 32\,\mathrm{kg\,m^{-3}}$, $E = 35.3\,\mathrm{MPa}$, $G = 12.6\,\mathrm{MPa}$

PZT5H piezoelectric actuators
$\rho = 7500\,\mathrm{kg\,m^{-3}}$

$$\mathbf{c} = \begin{bmatrix} 126 & 79.5 & 84.1 & 0 & 0 & 0 \\ & 126 & 84.1 & 0 & 0 & 0 \\ & & 117 & 0 & 0 & 0 \\ & & & 23 & 0 & 0 \\ & & & & 23 & 0 \\ & & & & & 23 \end{bmatrix} \mathrm{GPa}$$

$$\mathbf{e} = \begin{bmatrix} 0 & 0 & 0 & 0 & 0 & 17 \\ 0 & 0 & 0 & 0 & 17 & 0 \\ -6.5 & -6.5 & 23.3 & 0 & 0 & 0 \end{bmatrix} \mathrm{Cm^{-2}}$$

Static Analysis

As a first analysis, the deflection of the sandwich beam when actuated by the pair of extension actuators and shear actuators is evaluated and compared. The deformed shape of the extension-actuated sandwich beam is shown in Figure 3 for three different cases. In the first case, only the left extension actuator is activated by a constant voltage (Figure 3(a)). In the second case, the same voltage is applied to both extension actuators (Figure 3(b)). In the third case, the extension actuators are subjected to voltages with the same magnitude, but with opposite signs for left and right actuators (Figure 3(c)). From these deformed shapes, it can be observed that, when applying the same voltage to both extension actuators, a symmetric deformation of the

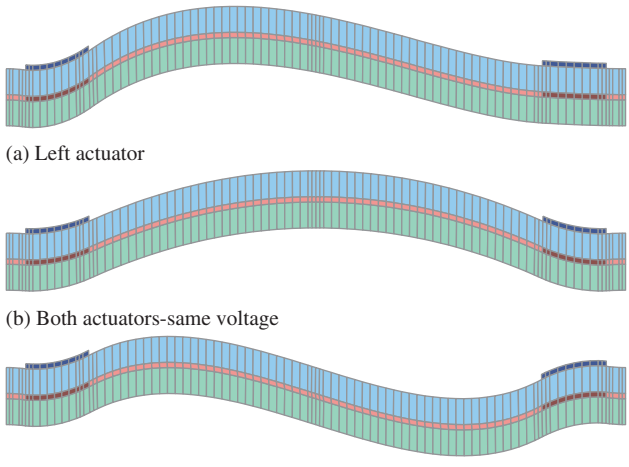

Figure 3. *Deformed configuration induced by static extension actuation.*

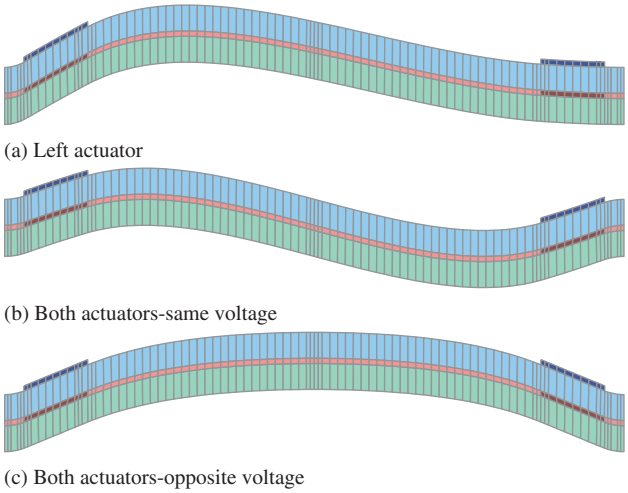

Figure 4. *Deformed configuration induced by static shear actuation.*

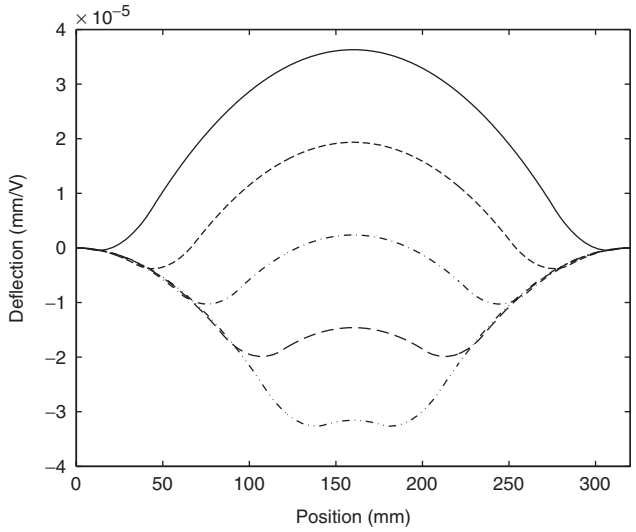

Figure 5. *Deformed configuration induced by equal unitary voltages applied to the extension actuators at several locations (d, in mm). —: 10, - - -: 35, –·–: 60, – –: 85, –···–: 110.*

sandwich beam is induced, but the application of opposite voltages induces an antisymmetric deformation. A similar analysis is now performed for the actuation through the shear actuators (Figure 4). Comparison of Figures 4(a) and 3(a) shows that shear actuation mechanism induces a similar deformation for a single actuator. Interestingly, the actuation behavior of two shear actuators located at the beam extremes is opposed to that of the extension actuators. In particular, the application of equal voltages to both of the shear actuators induces an antisymmetric deformation of the sandwich beam, while equal voltages with opposite signs induces a symmetric deformation.

As a second analysis, the effect of the actuators' position on the deformed shape and deflection magnitude of the sandwich beam is evaluated. This is carried out by varying the distance (d) between the actuators

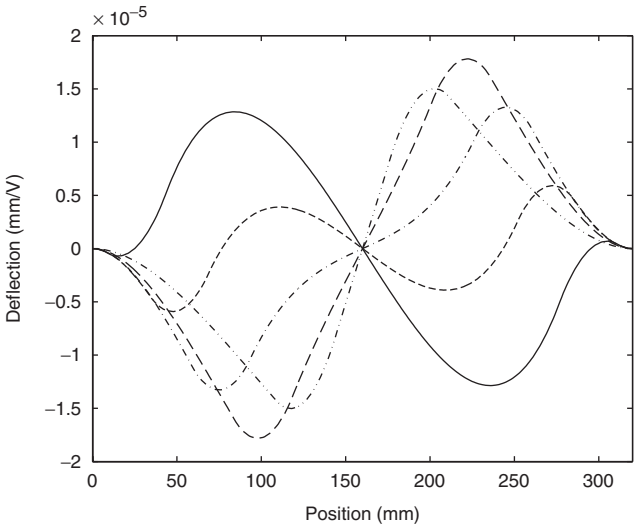

Figure 6. *Deformed configuration induced by opposite unitary voltages applied to the extension actuators at several locations (d, in mm). —: 10, - - -: 35, –·–: 60, – –: 85, –···–: 110.*

and the clamped ends and evaluating the deflection along the beam length induced by a unitary voltage applied to the extension and shear actuators (for both equal and opposite signs). This task effort was greatly simplified due to an automatic update of the finite element mesh.

In the first case, equal unitary voltages are applied to the extension actuators which were located at 10, 35, 60, 85, and 110 mm away from the clamped ends. From the analysis of the induced deflection shown in Figure 5, it can be observed that placing the actuators either near the clamped end or near the center of the beam leads to the most effective designs. It is worthwhile to also notice that, as expected, the deflection of the beam approaches the well-known shape of a clamped–clamped beam actuated by a single centered extension actuator as long as the two extension actuators converge to the center.

Then, the same parametric analysis is performed, and shown in Figure 6, for the extension actuators subjected to opposite voltages. As already observed, this actuation configuration leads to an antisymmetric deformation of the beam. However, due to the actuation mechanism of each extension actuator, the deformed shape may present quite complex forms. Indeed, for extension actuators near the clamped ends, the left side of the beam presents positive deflection while the right side presents negative deflection. On the contrary, as the extension actuators approach the beam center, the left side of the beam presents negative deflection while the right side presents positive deflection. Notice that in all cases, the deflection at the beam length mid-point is null.

As previously noted, the behavior of a pair of shear actuators located at the extremes of a clamped–clamped sandwich beam is opposite of that for extension actuators, that is, inducing antisymmetric deformation

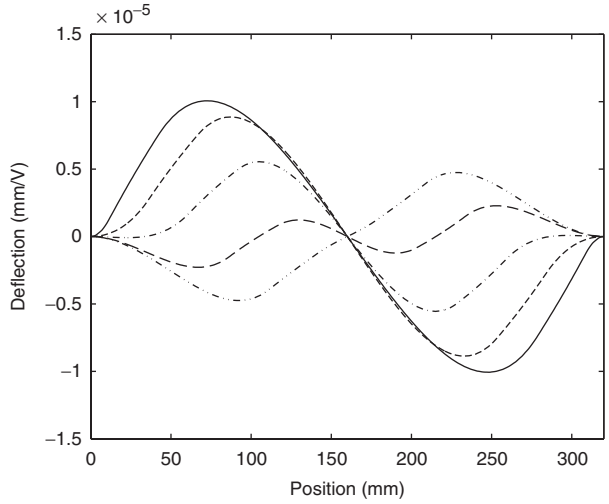

Figure 7. *Deformed configuration induced by equal unitary voltages applied to the shear actuators at several locations (d, in mm). —: 10, - - -: 35, –·–: 60, – –: 85, –··–: 110.*

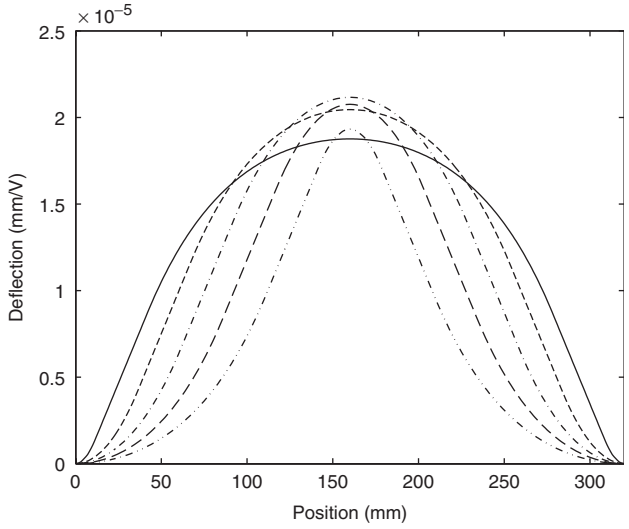

Figure 8. *Deformed configuration induced by opposite unitary voltages applied to the shear actuators at several locations (d, in mm). —: 10, - - -: 35, –·–: 60, – –: 85, –··–: 110.*

for equal voltages and symmetric deformation for opposite voltages. To better understand the shear actuation, an analysis of the effect of the actuators' position on the deformed shape and deflection magnitude was carried out. Figure 7 shows the deflection induced by equal unitary voltages applied to the shear actuators when these are located at 10, 35, 60, 85, and 110 mm away from the clamped ends. It can be observed that locating the shear actuators near the clamped end leads to the most effective design. Notice also that, just as for the extension actuators with opposite voltages, the deflection is always antisymmetric so that the mid-point of beam length presents no deflection.

When unitary voltages with opposite signs are applied to each shear actuator, a symmetric deformed shape is induced. Results from the parametric analysis for this case are shown in Figure 8. One important result from the parametric analysis that can be observed in Figure 8, is that the mid-point deflection is not very dependent on the actuators' position, although it is optimal for $d = 60$ mm. Thus, shear actuators may be an interesting alternative design for actuation of clamped–clamped beams when mid-point deflection and actuators' location are important issues. On the other hand, it is also worthwhile noting that the deflection shape of sandwich beams actuated by shear actuators near the beam center is very similar to that obtained when using single extension actuators at the beam center.

Active Damping Performance

In this section, the reduced model joined with the limited input optimal control strategy presented previously is applied to an active damping performance analysis of the shear and extension actuation applied to the clamped–clamped sandwich beam. In particular, three specific cases are analyzed: actuation through extension actuators only, actuation through shear actuators only, and actuation through combined extension and shear actuation. For all cases, geometric and material properties are those presented in Table 1, i.e., for actuators located near the clamped ends. Also, for pure extension actuation, shear actuators are inactive so that they act as elastic layers and vice versa.

The first 15 vibration modes are considered to build the reduced model used in the present analysis. To obtain a fine representation of higher modes, 93 variable-length piezoelectric laminate/sandwich beam finite elements are used, leading to an average element length of 3.4 mm. For comparison purposes, the viscous damping matrix is defined so that a passive modal damping factor of 1% is obtained for all bending modes. The control design is carried out using the iterative LQR algorithm with unitary state and input weight matrices. The control gain matrix $\mathbf{K}_g$ is then evaluated for a transverse perturbation force applied on the mid-point of the beam, such that the maximum deflection amplitude is 0.1 mm and the maximum voltage applied to the actuators is 250 V, i.e., an electric field of 500 V/mm. Notice that for shear, extension, and combined extension–shear actuation, the voltages applied to each piezoelectric actuator are independent. Hence, the input signal is composed of two independent voltages for pure extension and shear actuation, and four independent voltages for combined extension–shear actuation. In the case of combined actuation, however, since shear and extension actuation mechanisms lead to different input distribution vectors, the input weight matrix $\mathbf{R}$ was modified to guarantee maximum voltage on both extension and shear actuators.

Table 2. Modal damping factors (%) of the sandwich beam with extension, shear and combined actuation.

	ζ_1	ζ_2	ζ_3	ζ_4	ζ_5	ζ_6	ζ_7	ζ_8	ζ_9	ζ_{10}	ζ_{11}	ζ_{12}	ζ_{13}	ζ_{14}	ζ_{15}
Extension	3.2	2.9	2.3	1.7	1.1	1.1	1.5	2.0	2.4	2.7	2.7	3.1	3.1	2.5	1.2
Shear	2.1	2.4	2.7	2.6	2.7	2.0	2.1	1.5	1.3	1.4	1.0	1.2	1.5	1.1	1.8
Hybrid	4.5	4.2	4.2	3.6	3.0	2.5	2.5	2.8	3.1	3.4	3.2	3.8	3.9	3.0	2.3

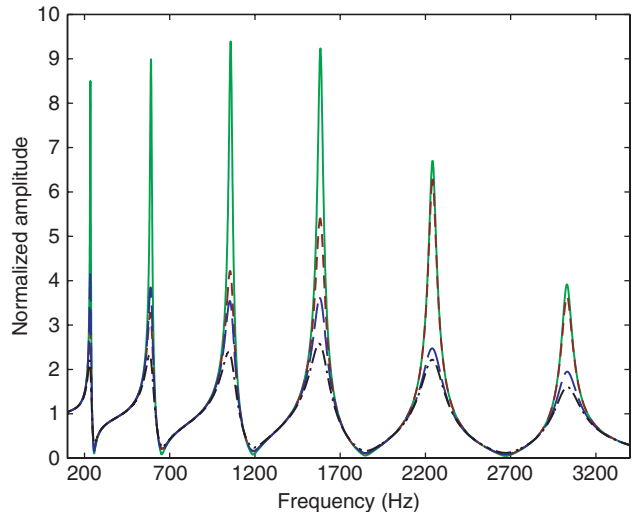

Figure 9. *Frequency response of the sandwich beam with extension and shear actuators located at the beam extremes. —: without control, - - -: extension actuation, – –: shear actuation, –·–: combined actuation.*

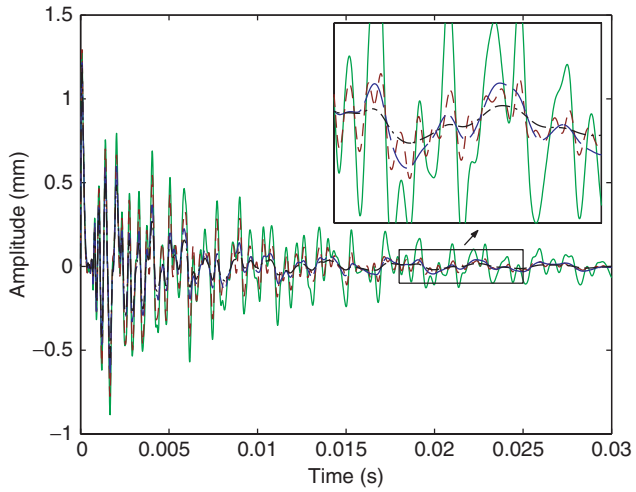

Figure 10. *Impulse response of the sandwich beam with extension and shear actuators located at the beam extremes. —: without control, - - -: extension actuation, – –: shear actuation, –·–: combined actuation.*

This was achieved by considering $\mathbf{R}$ to be in the form $\mathbf{R} = \gamma\,(1, 1, R_s, R_s)$, where R_s refers to the weight of the voltages applied to the shear actuators and was manually adjusted, and γ was evaluated by the iterative control algorithm.

To evaluate the active damping performance, time and frequency responses of the sandwich beam were evaluated for four cases: without control, with extension actuation only, with shear actuation only, and with combined extension–shear actuation. For clarity purposes, the responses shown here were obtained using a transverse point force applied at 40 mm from the clamped end as the excitation, and the deflection at the same point as the measured response. As it can be observed in Figure 9, both extension and shear actuators are able to damp the first six vibration modes considerably. However, the extension actuation is more effective for the first three modes while the shear actuation presents an almost uniform performance within this frequency-range (150–3200 Hz). To facilitate the comparison, the modal damping factors of the first 15 vibration modes are presented in Table 2. However, the more important fact is that the combined extension–shear actuation greatly outperforms both extension and shear actuation alone for all the 15 modes, as shown both in Figure 9 and Table 2. There is one nontrivial reason for this performance, besides the more obvious fact that there are four active actuators instead of only two. In fact, extension and shear actuation mechanisms are complementary, so that for modes where one of them has poor performance the other counterbalances with a better performance. Indeed, one may observe in Table 2 that, while some modes are not well-damped by extension or shear actuation alone (e.g., 5th/6th modes for extension and 11th/14th for shear actuation), all modes are well damped by the combined extension–shear actuation. This can also be observed in the time response (Figure 10), where one can notice that the shear actuation dampens well the higher frequency oscillations. This effect is then combined to the low-frequency damping of extension actuation, leading to smaller vibration amplitude for the combined extension–shear actuation. Notice that this yields a good damping performance over an increased frequency-range with very localized actuators, that is, without the need to spread actuators along the beam length. This characterizes one of the greatest advantages of combining these two complementary actuation mechanisms.

CONCLUSIONS

The first results of a numerical investigation of active vibration control using simultaneous extension and

shear piezoelectric actuation for a clamped–clamped sandwich beam were presented in this work. First, using a laminate/sandwich beam finite element model, a static analysis was carried out to better understand the actuation mechanisms of extension and shear piezoelectric actuators. Results have shown that, for clamped–clamped beams with shear actuation, the deflection is not very dependent on the actuators' position. Thus, shear actuators may be an interesting alternative design for actuation of clamped–clamped beams when the actuators' location is restricted. Then, combining the reduced finite element model to an optimal control algorithm with limited input, a selected configuration was tested to evaluate the active damping performance of extension, shear, and combined extension–shear actuators. Results have shown that simultaneous use of extension and shear actuators is very promising since extension and shear actuation mechanisms are complementary, so that for modes where one of them has poor performance, the other counterbalances with a better performance. Therefore, one of the greatest advantages of a combined extension–shear actuation is that a good damping performance can be obtained over an increased frequency range with very localized actuators. Notice that the active damping performance obtained is valid for the clamped–clamped sandwich beam studied here. However, it seems that the combination of extension and shear actuations could also be advantageous for other boundary conditions since it provides two different actuation mechanisms at the same time. The combination of active damping, through extension and shear actuation, and passive viscoelastic damping treatments is being considered for future work.

ACKNOWLEDGMENTS

Support of the State of São Paulo Research Foundation (FAPESP), through research grant 04/10255-7, is gratefully acknowledged.

REFERENCES

Ahmadian, M. and DeGuilio, A.P. 2001. "Recent Advances in the Use of Piezoceramics for Vibration Suppression," *The Shock and Vibration Digest*, 33(1):15–22.

Aldraihem, O.J. and Khdeir, A.A. 2000. "Smart Beams with Extension and Thickness-shear Piezoelectric Actuators," *Smart Materials and Structures*, 9(1):1–9.

Aldraihem, O.J. and Khdeir, A.A. 2003. "Exact Deflection Solutions of Beams with Shear Piezoelectric Actuators," *International Journal of Solids and Structures*, 40(1):1–12.

Baillargeon, B.P. and Vel, S.S. 2005. "Active Vibration Suppression of Sandwich Beams using Piezoelectric Shear Actuators: Experiments and Numerical Simulations," *Journal of Intelligent Material Systems and Structures*, 16(6):517–530.

Benjeddou, A., Trindade, M.A. and Ohayon, R. 1997. "A Unified Beam Finite Element Model for Extension and Shear Piezoelectric Actuation Mechanisms," *Journal of Intelligent Material Systems and Structures*, 8(12):1012–1025.

Benjeddou, A., Trindade, M.A. and Ohayon, R. 1999. "New Shear Actuated Smart Structure Beam Finite Element," *AIAA Journal*, 37(3):378–383.

Benjeddou, A., Trindade, M.A. and Ohayon, R. 2000. "Piezoelectric Actuation Mechanisms for Intelligent Sandwich Structures," *Smart Materials and Structures*, 9(3):328–335.

Edery-Azulay, L. and Abramovich, H. 2004. "Piezoelectric Actuation and Sensing Mechanisms – Closed Form Solutions," *Composite Structures*, 64(3–4):443–453.

Khdeir, A.A. and Aldraihem, O.J. 2001. "Deflection Analysis of Beams with Extension and Shear Piezoelectric Patches using Discontinuity Functions," *Smart Materials and Structures*, 10(2):212–220.

Raja, S., Prathap, G. and Sinha, P.K. 2002. "Active Vibration Control of Composite Sandwich Beams With Piezoelectric Extension-bending and Shear Actuators," *Smart Materials and Structures*, 11(1):63–71.

Raja, S., Sreedeep, R. and Prathap, G. 2004. "Bending Behavior of Hybrid-actuated Piezoelectric Sandwich Beams," *Journal of Intelligent Material Systems and Structures*, 15(8):611–619.

Sun, C.T. and Zhang, X.D. 1995. "Use of Thickness-shear Mode in Adaptive Sandwich Structures," *Smart Materials and Structures*, 4(3):202–206.

Sunar, M. and Rao, S.S. 1999. "Recent Advances in Sensing and Control of Flexible Structures via Piezoelectric Materials Technology," *Applied Mechanics Review*, 52(1):1–16.

Trindade, M.A. and Benjeddou, A. 2002. "Hybrid Active-passive Damping Treatments using Viscoelastic and Piezoelectric Materials: Review and Assessment," *Journal of Vibration and Control*, 8(6):699–746.

Trindade, M.A., Benjeddou, A. and Ohayon, R. 1999. "Parametric Analysis of the Vibration Control of Sandwich Beams Through Shear-based Piezoelectric Actuation," *Journal of Intelligent Material Systems and Structures*, 10(5):377–385.

Trindade, M.A., Benjeddou, A. and Ohayon, R. 2001. "Finite Element Modeling of Hybrid Active-passive Vibration Damping of Multilayer Piezoelectric Sandwich Beams – Part 1: Formulation and Part 2: System Analysis," *International Journal for Numerical Methods in Engineering*, 51(7):835–864.

Vel, S.S. and Batra, R.C. 2001. "Exact Solution for the Cylindrical Bending of Laminated Plates with Embedded Piezoelectric Shear Actuators," *Smart Materials and Structures*, **10**(2):240–251

Zhang, X.D. and Sun, C.T. 1996. "Formulation of an Adaptive Sandwich Beam," *Smart Materials and Structures*, 5(6):814–823.